

Near-IR Spectroscopy of OH/IR stars in the Galactic Centre

E. Vanhollebeke¹, J.A.D.L. Blommaert¹, M. Schultheis², B. Aringer³, and A. Lançon⁴

¹ Instituut voor Sterrenkunde, K.U.Leuven, Celestijnenlaan 200B, B-3001 Leuven, Belgium

² CNRS UMR6091, Observatoire de Besançon, BP1615, F-25010 Besançon, France

³ Institut für Astronomie, Türkenschanzstrasse 17, A-1180 Wien, Austria

⁴ Observatoire Astronomique, Rue de L'Université 11, F-67000 Strasbourg, France

Received / Accepted

ABSTRACT

Context. Galactic Centre (GC) OH/IR stars can be, based on the expansion velocities of their circumstellar shells, divided into two groups which are kinematically different and therefore are believed to have evolved from different stellar populations.

Aims. To study the metallicity distribution of the OH/IR stars population in the GC on basis of a theoretical relation between EW(Na), EW(Ca) and EW(CO) and the metallicity.

Methods. For 70 OH/IR stars in the GC, we obtained near-IR spectra. The equivalent line widths of Na I, Ca I, ¹²CO(2,0) and the curvature of the spectrum around 1.6 μ m due to water absorption are determined.

Results. The near-IR spectrum of OH/IR stars is influenced by several physical processes. OH/IR stars are variable stars suffering high mass-loss rates. The dust that is formed around the stars strongly influences the near-IR spectra and reduces the equivalent line widths of Na I, Ca I. A similar effect is caused by the water content in the outer atmosphere of the OH/IR star. Because of these effects, it is not possible with our low resolution near-infrared spectroscopy to determine the metallicities of these stars.

Key words. Stars: AGB and post-AGB – Stars: late-type – Stars: mass-loss – Galaxy: bulge – Galaxy: center – Infrared: stars

1. Introduction

The inner region of our Galaxy has been extensively searched for OH/IR stars in the past two decades. The studies of the GC region are severely hampered, especially in the visible wavelength range, by extinction and also source confusion. Searches for OH/IR stars at radio wavelengths at the 1612 MHz OH maser line were therefore very useful and also provided kinematic information of the detected stars. Lindqvist et al. (1992b) searched for OH/IR stars in six VLA primary beam fields and identified 134 OH/IR stars. Further searches, also using ATCA, were conducted by Sevenster et al. (1997), who found 145 new OH masering sources in the Bulge and Sjouwerman et al. (1998) who discovered an additional 52 new OH/IR stars in the GC region. A review on Asymptotic Giant Branch (AGB) stars in the GC region can be found in Habing & Whitelock (2003).

Lindqvist et al. (1992a) studied the spatial and kinematic properties of their OH/IR sample and divided the stars into two groups on basis of their outflow velocities. OH/IR stars with small expansion velocities ($v_{\text{exp}} < 18.0$ km/s) have a larger spread in latitude and a larger velocity dispersion with respect to the galactic rotation than the group with higher expansion

velocities. This was also found by Baud et al. (1981) for OH/IR stars in the galactic disk. The low expansion velocity stars are expected to be older objects with larger peculiar motions, whereas the other group may have a different formation history; it might be a later addition to the GC, possibly via a merger. The outflow velocity of the circumstellar shell is related to the luminosity of the star and to the properties of the dust in the circumstellar shell (Habing et al. 1994; Elitzur et al. 2003).

Several groups have been searching for the infrared counterparts of the OH maser sources (Jones et al. 1994; Blommaert et al. 1998; Wood et al. 1998; Ortiz et al. 2002). It would be expected that the 'older' stars have lower luminosities than the high expansion group. Blommaert et al. (1998) found that the high expansion velocities group contains higher luminosity stars but that there was also a large overlap in the luminosity distributions of the 2 groups. Ortiz et al. (2002) also compared the measured luminosities using a larger number of stars and did not find any evidence for a distinction on basis of luminosities between the 2 groups. The disadvantage of the latter study is the fact that the luminosities were not corrected for variability and that the luminosities spread over a larger range. Nevertheless, it seems that the differences in luminosities between the 2 groups, if they exist, are not very strong. If the luminosity is not sufficient to explain the

differences in expansion velocities than it would be expected that differences in the gas to dust ratios and thus metallicities of the stars must exist. It was demonstrated by Wood et al. (1992) for OH/IR stars in the Large Magellanic Cloud and by Blommaert et al. (1993) for OH/IR stars in the outer Galaxy that the expansion velocities are low, even though the OH/IR stars have high luminosities. In both, the LMC and in the outer Galaxy, it is expected that the stars have indeed low metallicities. The next logical step would be to investigate the metallicities of GC OH/IR stars.

Schultheis et al. (2003) obtained near-IR spectra of 107 sources with mid-infrared excess selected from the ISOGAL survey (Omont et al. 2003), including 15 OH/IR sources. With an empirical formula based on near infrared spectroscopy of K and M giants (Ramírez et al. 2000; Frogel et al. 2001), Schultheis et al. (2003) tentatively estimated $[\text{Fe}/\text{H}]$ for all of the ISOGAL sources. Although Schultheis et al. (2003) indicate that the Ramírez et al. (2000) formula does not actually measure metallicity for an individual spectrum of a strongly variable star, it was found that it might still be used to find an average metallicity.

In this paper we will discuss our attempt to apply the results of Schultheis et al. (2003) on medium-resolution near-IR spectra on a sample of GC OH/IR stars. Three things will be discussed: we will take a look at the influence of the water content on the atomic lines Na I and Ca I , we discuss how periodicity can have an influence on the water content and therefore also influences the near-IR spectrum and we will study a grid of dust models and show that hot dust also has an influence on the near-IR spectrum.

The sample, observations and data-reduction will be described in the next section. In section 3, we explain our method of analyse and compare spectra we have in common with other authors. The problems one encounters analysing near-IR spectra of OH/IR stars will be discussed in section 4. Finally in section 5 we summarise and come to the conclusions.

2. Observations and data reduction

2.1. Sample

The sample consists of 70 OH/IR stars located in the GC region. Almost all stars are selected from Lindqvist et al. (1992b) and Sjouwerman et al. (1998). Our sample also includes the 15 OH/IR stars observed by Schultheis et al. (2003) so that we can compare our results and investigate the effect of the variability of this type of stars. We also selected the three "high-velocity" OH/IR stars that were detected in the direction of the GC (van Langevelde et al. 1992). As we wanted to apply the metallicity versus $\text{EW}(\text{Na})$, $\text{EW}(\text{Ca})$ and $\text{EW}(\text{CO})$ calibration used in Ramírez et al. (2000) and Frogel et al. (2001) to our sample we also observed 11 stars from Ramírez et al. (1997) (K-band spectra of 43 luminosity class III stars from K0 to M6) and Ramírez et al. (2000) (K-band spectra of more than 110 M giants in the Galactic Bulge (GB)). Finally, to investi-

gate the effects of the variability of our Long Period Variable stars (LPVs) on our analysis we measured variable stars from Lançon & Wood (2000) (spectra of cool, mostly variable, giant and supergiant stars) (see Table A.1 – Table A.3).

2.2. Observations

The near-IR spectra were obtained with the 3.58 m NTT (ESO) at la Silla, Chile between June 28th - 30th 2003 using the red grism of the SOFI spectrograph. This resulted in spectra from $1.53 \mu\text{m}$ up to $2.52 \mu\text{m}$. Before the actual spectrum was obtained, the instrument was used in imaging mode, to acquire the star in the slit. Several spectra were taken with the star in different places along the slit. Standard stars of spectral type O till G were observed as close as possible to the object stars' airmass in order to correct for telluric absorption features.

2.3. Data reduction

The data reduction was done using the ESO-Munich Image Data Analysis System (ESO-MIDAS). The images were first corrected for cosmic ray hits. Several spectra of the same target along the slit were obtained and subtracted from each other to correct for the sky level. The images were flat-fielded using dome flats. A Gaussian fit perpendicular to the dispersion direction was used to subtract a one dimensional spectrum out of the two dimensional image: columns that fall within the FWHM of the Gaussian fit were added to the spectrum (3-4 columns on average). A correction for distortion along the slit was unnecessary. During the extraction process, a correction for bad pixels was made, they were left out of the spectrum, no averaging was done around these pixels. The wavelength calibration was based on the spectrum of a Xenon lamp. This image was also flat-fielded using the dome flats and corrected for bad pixels in the same way as the other spectra. The wavelength calibration resulted in a dispersion of typically $10.13 \text{ \AA}/\text{pixel}$ and $\lambda/\Delta\lambda \approx 1000$.

The standard stars were reduced in the same way. Thereafter they were divided by a Kurucz-model that corresponds to their spectral type. The resulting curve was used to correct the objects for telluric lines and also to correct for the instrumental response function. Different curves for different airmasses were made in order to correct for the airmass.

The dereddening law used, is based on Cardelli et al. (1989), A_v values came from Schultheis et al. (1999).

The resulting spectra are shown in Fig. B.1 till Fig. B.8.

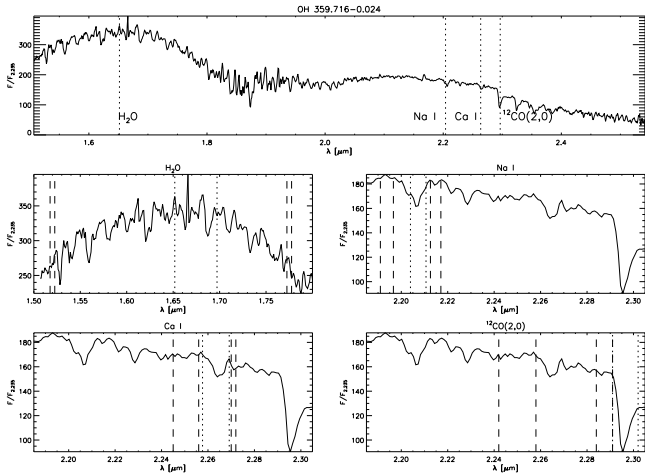
3. Analysis

3.1. Equivalent line widths

The equivalent line widths of Na I , Ca I and $^{12}\text{CO}(2,0)$ (see Tables A.1 – A.3) were obtained in exact the same way as by Schultheis et al. (2003) (see also Ramírez et al. 1997; Lançon & Wood 2000). They were measured relative to the selected continuum bands using the Image Reduction and Analysis Facility (IRAF) (see Table 1 and Fig. 1).

Table 1. Definition of band passes for continuum and features (Schultheis et al. 2003).

Feature	Band passes [μm]
Na I feature	2.204 – 2.211
Na I continuum #1	2.191 – 2.197
Na I continuum #2	2.213 – 2.217
Ca I feature	2.258 – 2.269
Ca I continuum #1	2.245 – 2.256
Ca I continuum #2	2.270 – 2.272
$^{12}\text{CO}(2,0)$ feature band head	2.289 – 2.302
$^{12}\text{CO}(2,0)$ continuum #1	2.252 – 2.258
$^{12}\text{CO}(2,0)$ continuum #2	2.284 – 2.291
H_2O continuum	1.629 – 1.720
H_2O absorption wing 1	1.515 – 1.525
H_2O absorption wing 2	1.770 – 1.780

**Fig. 1.** An overview of the chosen definition of band passes for continuum and features. The top figure shows the overall spectrum for a typical OH/IR stars. The dotted lines indicate the central positions of the features. The other 4 figures show for each line the selected passband for the feature (dotted lines) and the selected passband for the continuum (dashed lines). (For the $^{12}\text{CO}(2,0)$ the feature's first dotted line overlaps with the last dashed line from the continuum.)

Ramírez et al. (1997) discuss how the equivalent width measurements of Na I and Ca I in medium resolution spectra contain contributions from other elements such as Sc, Ti, V, Si and S. Thus, it turns out that a significant contribution of the Na I and Ca I features is due to other species. In the studied spectral region (1.53–2.52 μm) the CN molecule causes a noisy continuum (Origlia et al. 1993), introducing a pseudo-continuum opacity (this is clearly shown in the high-resolution spectrum of RX Boo (an M8 III star) in Wallace & Hinkle (1996)). According to Ramírez et al. (1997) the continuum bands that were used to determine the EW(Ca) get affected by CN absorption for stars with $T_{\text{eff}} < 3000$ K. However, synthetic CN spectra based on hydrostatic MARCS models for giant stars (for a description of such models see Aringer et al. (1997), in our case we assumed $\log(G [\text{cm/s}^2]) = 0.0$, solar mass and elemental abundances) show that CN is important in all cool

objects below 4000 K, and even gets weaker below 3000 K.

The effective temperature has a strong impact on the Ca I and Na I features: as T_{eff} decreases, the equivalent widths of both features increase. Tables A.4, A.5 and A.6 give an overview of what the respectively Na I, Ca I and $^{12}\text{CO}(2,0)$ lines in a medium resolution spectrum are really made of. The tables are based on the high-resolution spectrum of RX Boo in Wallace & Hinkle (1996). For cooler oxygen-rich stars (Lançon & Wood 2000), such as OH/IR stars, H_2O absorption, instead of CN absorption, becomes very important (see section 4.3).

3.2. Water absorption

The amount of water has been obtained by measuring the curvature in the spectrum around 1.6 μm , as in Schultheis et al. (2003). The apparent bump around 1.6 μm is caused by strong and wide water absorption bands around 1.4 and 1.9 μm . Formally, our measurements are equivalent widths of this bump relative to reference fluxes measured on either side of it in the wings of the water bands. As for the other equivalent line width measurements, its value is given in \AA , but it takes negative values when water absorption is present (see Tables A.1 – A.3).

3.3. Comparison with previous work

We have 5 candidate Red Giant Branch (RGB) stars in common with Schultheis et al. (2003). These candidate RGB stars, are likely genuine ones, since we see no significant difference between Schultheis et al. (2003) observations of these stars and our observations. Stars on the RGB are expected to show weak variations compared to OH/IR stars and Miras.

Schultheis et al. (2003) observed the stars with the same instrument (SOFI), using the same grism. This results in spectra with the same resolution as our spectra. The time difference between these observations is about 3 years. The spectra (normalised at 2.235 μm) are compared in Fig. 2 and Table 2 gives the mean values and standard deviations for the stars we have in common. The absolute average differences in equivalent line widths for these RGB stars are consistent with scatter due to formal errors ($\sim 1 \text{\AA}$). One expects these errors to come from data-reduction issues, stability of observing conditions during the night. The absolute average differences are: $0.25 \pm 0.17 \text{\AA}$ for EW(Na), $0.72 \pm 0.42 \text{\AA}$ for EW(Ca) and $0.87 \pm 0.82 \text{\AA}$ for EW(CO) (see also Fig. 3).

We have 8 late-type giants in common with Ramírez et al. (1997) and 6 red giants situated in the Bulge with Ramírez et al. (2000). A comparison was made only for EW(Na) and EW(Ca), since Ramírez et al. (1997) uses different continuum pass bands for obtaining EW(CO). Tables 3 and 4 give the mean values for the compared equivalent line widths. The absolute average differences with Ramírez et al. (1997) are: $0.39 \pm 0.13 \text{\AA}$ for EW(Na) and $1.29 \pm 0.41 \text{\AA}$ for EW(Ca). The absolute average differences with Ramírez et al. (2000) are $0.59 \pm 0.23 \text{\AA}$ for EW(Na) and $0.66 \pm 0.35 \text{\AA}$ for EW(Ca). The difference in EW(Na) (Ramírez et al. 1997, 2000) and EW(Ca)

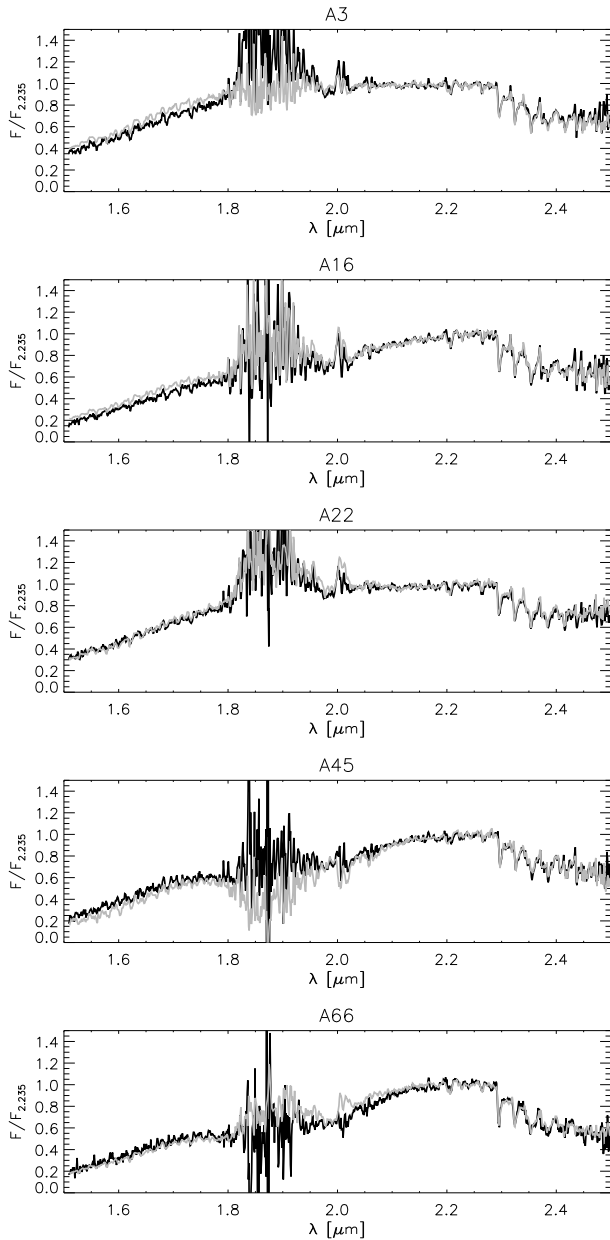


Fig. 2. RGB stars in common with Schultheis et al. (2003); black line: this work, gray line: Schultheis et al. (2003). The features between 1.8 and 1.9 μm and around 2 μm are due to the atmosphere.

(Ramírez et al. 2000) is again consistent with scatter due to formal errors. There is no obvious reason why the difference for $\text{EW}(\text{Ca})$ (Ramírez et al. 1997) is larger than $\sim 1 \text{ \AA}$ (see also Fig. 4), although we have to keep in mind that there is a difference in resolution between our spectra and the spectra of Ramírez et al. (1997, 2000), which can influence the difference between the measured equivalent line widths. The data from Ramírez et al. (2000) can be downloaded from the internet. After rebinning the data to our lower resolution, the following values could be measured: 3.95 ± 0.78 for the $\text{EW}(\text{Na})$ and 2.77 ± 0.47 for the $\text{EW}(\text{Ca})$, which resembles better the values

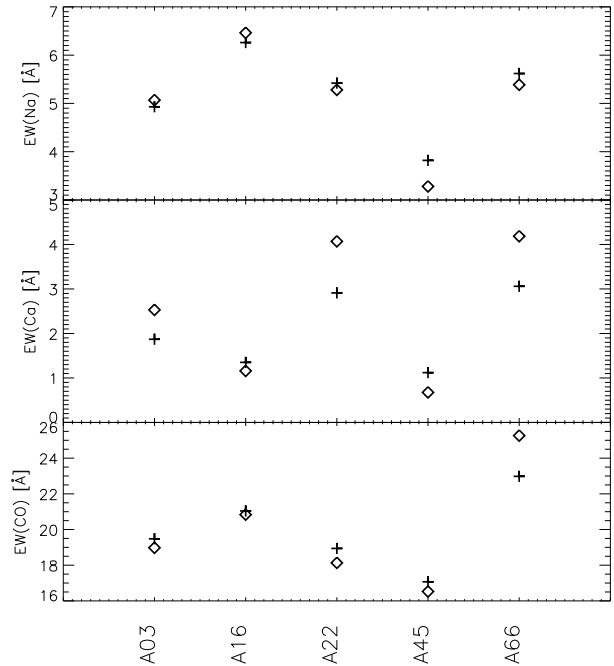


Fig. 3. Equivalent line width measurements for the candidate RGB stars in common with Schultheis et al. (2003). The plus-signs are taken from Schultheis et al. (2003), the diamonds from this work.

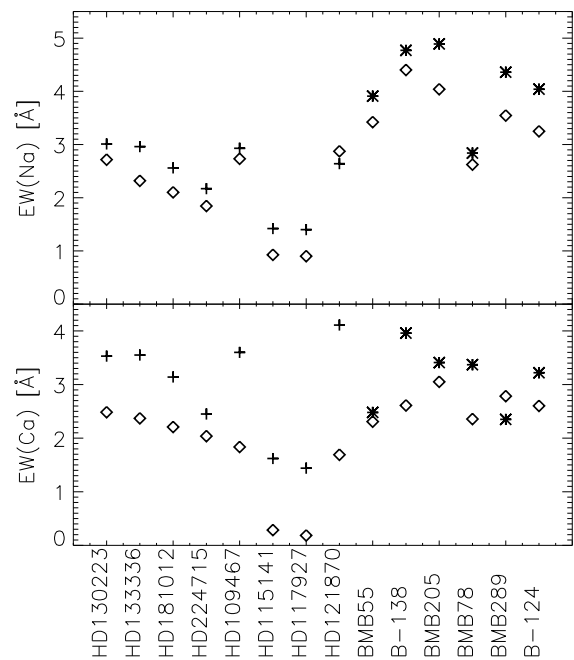


Fig. 4. Equivalent line width measurements for the stars in common with Ramírez et al. (1997) and Ramírez et al. (2000). The plus-signs are taken from Ramírez et al. (1997), the stars are from Ramírez et al. (2000) and the diamonds are from this work.

we found (see Table 3). A similar test for Ramírez et al. (1997) could not be done.

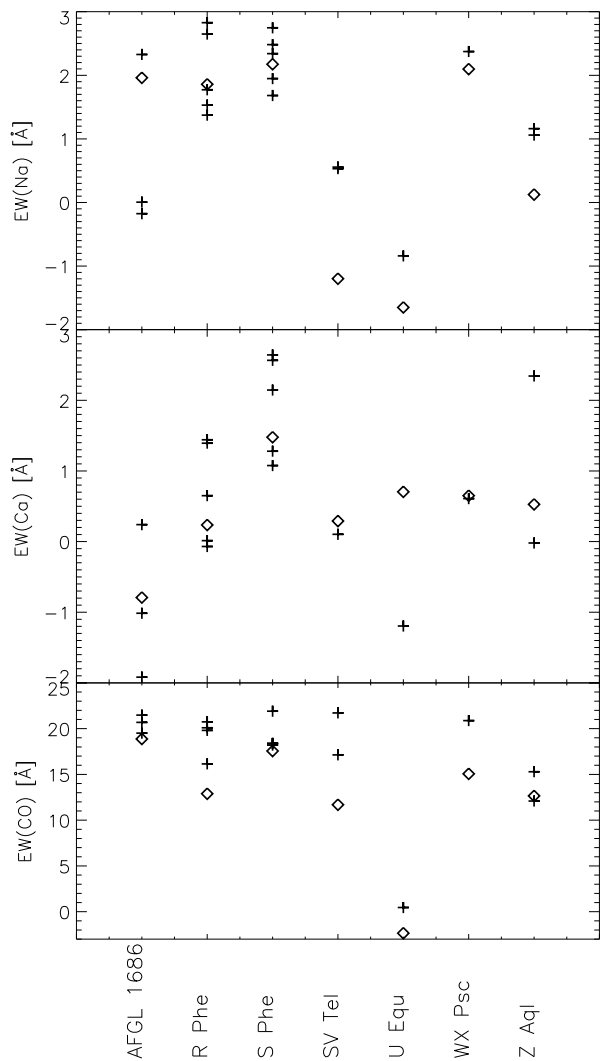


Fig. 5. Variations in the equivalent widths for stars in common with Lançon & Wood (2000). The plus-signs are taken from Lançon & Wood (2000), the diamonds from this work.

We have 7 luminous cool stars in common with Lançon & Wood (2000). Three of these stars (WX Psc, AFGL 1686 and U Equ) are OH/IR stars (Lançon & Wood 2000). These OH/IR stars (not situated in the GC) are used as a comparison for the equivalent line width measurements. The other 4 stars, have periods in the range from 120 to 270 days. Some of the stars were observed several times by Lançon & Wood (2000). The differences in equivalent line widths between the measurements based on the available spectra of Lançon & Wood (2000) and our measurements are shown in Fig. 5. The differences seen in this plot, are large in comparison with the differences seen in Fig. 3 and Fig. 4, especially for EW(CO), and can't be explained only by formal errors. The variability of the stars is responsible for the large variations in the equivalent line widths (see section 4.4). Our measured equivalent line widths do fall within the range of equivalent line widths based on the spectra of Lançon & Wood (2000) (see Fig. 5). We can expect that the OH/IR stars that we have in common with Schultheis et al. (2003) will show simi-

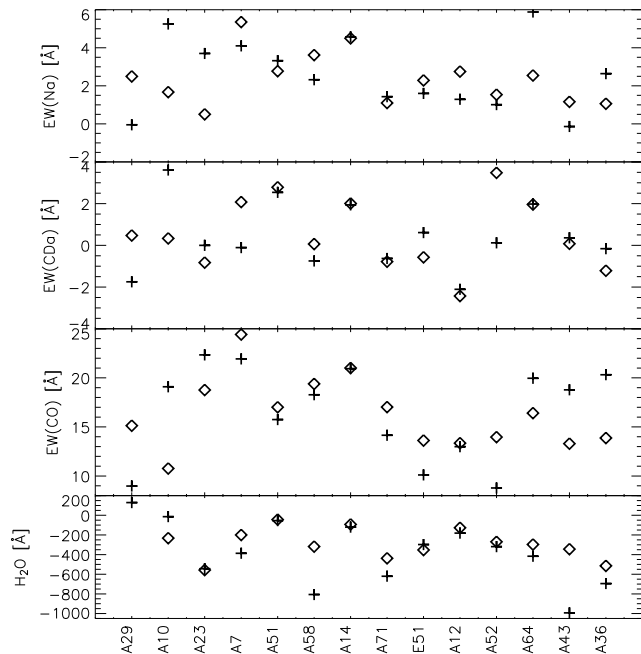


Fig. 6. Equivalent line width measurements for the OH/IR stars in common with Schultheis et al. (2003). The plus-signs are taken from Schultheis et al. (2003), the diamonds are from this work.

Table 2. Mean values for the equivalent line widths for the stars in common with Schultheis et al. (2003).

	this work	Schultheis et al. (2003)
Na I	5.10 ± 0.74	5.21 ± 0.67
Ca I	2.52 ± 1.29	2.06 ± 0.74
$^{12}\text{CO}(2,0)$	19.95 ± 2.48	19.90 ± 1.69

Table 3. Mean values for the equivalent line widths for the stars in common with Ramírez et al. (1997).

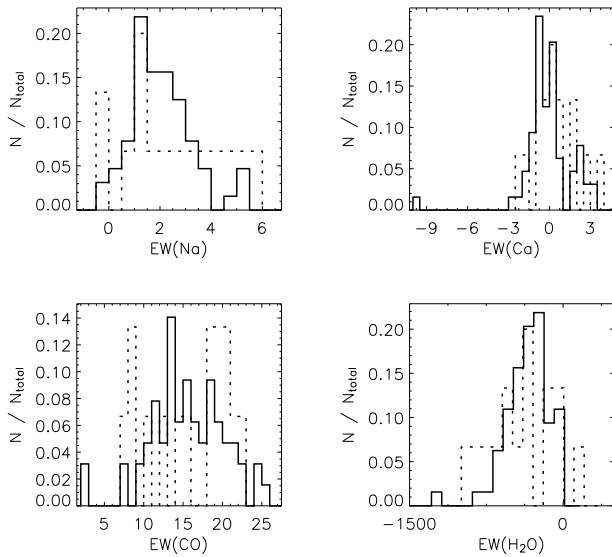
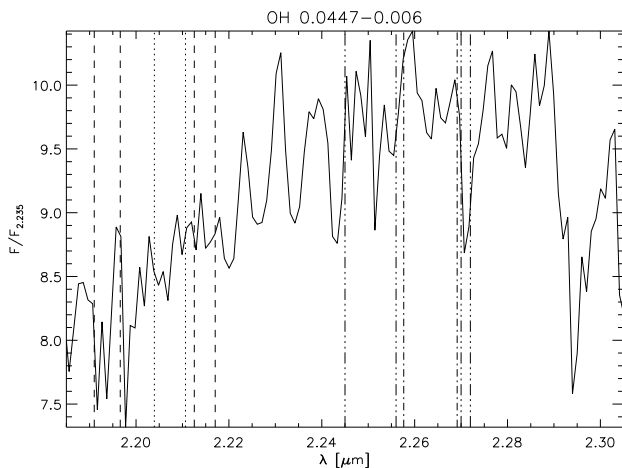
	this work	Ramírez et al. (1997)
Na I	2.05 ± 0.62	2.39 ± 0.54
Ca I	1.64 ± 0.70	2.93 ± 0.82

lar variations in their equivalent line widths, as is illustrated in Fig. 6. The mean absolute differences for the OH/IR stars in common with Schultheis et al. (2003) concerning the equivalent line widths are: 1.56 ± 1.17 Å for EW(Na), 1.14 ± 1.16 Å for EW(Ca), 3.60 ± 2.47 Å for EW(CO) and 171.81 ± 193.03 Å for the water absorption. These variations are caused by the variability of these OH/IR stars, as will be explained in the following section.

Fig. 7 gives an overview of the equivalent line widths for Na I, Ca I and $^{12}\text{CO}(2,0)$ (see section 3.1 and Table 1). The fourth histogram gives also the amount of water. Only the OH/IR stars are considered in this figure. Notice that the EW(Na), EW(Ca), EW(CO) and the EW(H₂O) are all in the same unit Å. The EW(H₂O) are all negative values, indicating

Table 4. Mean values for the equivalent line widths for the stars in common with Ramírez et al. (2000).

	this work	Ramírez et al. (2000)	Ramírez et al. (2000) after rebinning
Na I	3.55 ± 0.45	4.13 ± 0.54	3.95 ± 0.78
Ca I	2.62 ± 0.20	3.13 ± 0.48	2.77 ± 0.47

**Fig. 7.** Histograms for EW(Ca), EW(Na), EW(CO) and the water absorption for the OH/IR stars from this work (full line) and the OH/IR stars from Schultheis et al. (2003) (dotted line). All x-axes are in the same unit Å.**Fig. 8.** OH/IR star for which the Na I and Ca I lines couldn't be measured. The dotted lines indicate the Na I feature and the dashed lines the selected continuum points. The dashed-dotted lines indicate the Ca I feature with its corresponding continuum (dashed-triple-dotted).

water absorption in the spectrum around $1.6 \mu\text{m}$, as can be seen from the spectra of the OH/IR stars in Figure B.1. A negative value for EW(Ca) and EW(Na), indicates that the line couldn't be measured, we do not expect these lines in emission. Fig 8 gives an example of this. Especially for Ca I it is clear why the feature couldn't be measured: the second continuum band pass shows a very deep feature, which causes the flux measurement in the feature to be higher than in the continuum. This is also the case for the Na I feature, but here the first continuum band pass causes it (less clear than for the Ca I feature).

Fig. 2 in Ramírez et al. (2000) gives a $1 - 5 \text{ \AA}$ range for EW(Ca) and a $2 - 6 \text{ \AA}$ range for EW(Na) for a sample of red giants in the GB. Fig. 7 shows that our ranges for the equivalent widths for both Ca I and Na I are lower. Histograms for the equivalent line widths of Na I, Ca I and $^{12}\text{CO}(2,0)$ and the water amount for the 15 OH/IR stars in Schultheis et al. (2003) is also shown in Fig. 7 (dotted line). Their average equivalent widths are: $0.42 \pm 1.56 \text{ \AA}$ for EW(Ca), $2.50 \pm 1.90 \text{ \AA}$ for EW(Na) and $16.01 \pm 5.16 \text{ \AA}$ for EW(CO). The equivalent widths for the OH/IR stars in this work are: $0.08 \pm 1.88 \text{ \AA}$ for EW(Ca), $2.11 \pm 1.27 \text{ \AA}$ for EW(Na) and $15.60 \pm 4.69 \text{ \AA}$ for EW(CO). The largest difference is seen for EW(Ca): a lot of the OH/IR stars in this work and in Schultheis et al. (2003) have no measurable Ca I lines.

4. Discussion

4.1. Metallicities of OH/IR stars in the GC

Schultheis et al. (2003) investigated the metallicity distribution of 107 ISOGAL sources in the GB. The sample consists of different types of stars: non-variable giants, OH/IR stars, supergiants and LPVs. The metallicity distribution is determined based on the equivalent line widths of Na I, Ca I and $^{12}\text{CO}(2,0)$ (see Ramírez et al. 2000; Frogel et al. 2001; Schultheis et al. 2003). The calibration of the relation is based on giants in globular clusters in the range $-1.8 < [\text{Fe}/\text{H}] < -0.1$. The mean $[\text{Fe}/\text{H}]$ value in Schultheis et al. (2003) is consistent with previous chemical abundance studies of the GB (Schultheis et al. 2003). Apparently variable stars, such as Miras and OH/IR stars, do not influence the peak in the metallicity distribution determined in Schultheis et al. (2003), although they might broaden the distribution.

Applying the results of Schultheis et al. (2003) to our sample of OH/IR stars could help to find a metallicity difference between the two different groups of OH/IR stars in the GC as discussed in the introduction.

The equivalent line widths of Na I, Ca I and $^{12}\text{CO}(2,0)$ are determined as described in section 3.1. The values, given in Tables A.1, A.2 and A.3, are given in Å. A positive value indicates absorption and a negative value indicates emission. Immediately one notices the rather large amount of negative values for EW(Ca). One does not expect the Ca I line and the Na I line to be in emission. Inspecting the spectra for these stars (Fig. B.1 until Fig. B.4) shows that for a lot of stars the Ca I lines seem to disappear in the continuum. This effect is

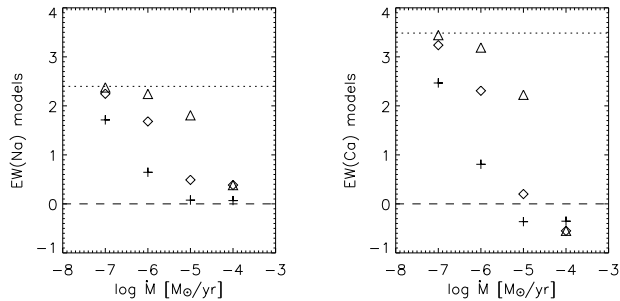


Fig. 9. Equivalent line widths for the different models. The x-axis indicates the mass-loss rate, the y-axis the equivalent line widths for Na I (left) and Ca I (right). The different symbols indicate the different dust temperatures. Crosses: $T_{dust} = 1500$ K, diamonds: $T_{dust} = 1000$ K and triangles: $T_{dust} = 750$ K. The dotted line indicates the equivalent line width for the reference line. The line disappears when the equivalent width is below the dashed line.

also noticeable for Na I in some stars.

In the rest of this section we will discuss the physical effects that can cause the Ca I and sometimes the Na I to appear apparently in emission.

4.2. Dust

OH/IR stars are AGB stars in their final phase on the AGB and are believed to be progenitors of Planetary Nebulae (e.g. Cohen et al. 2005; Habing 1996). OH/IR stars have high mass-loss rates between $\dot{M} = 10^{-6} M_{\odot}/\text{yr}$ and $10^{-4} M_{\odot}/\text{yr}$. It is not unlikely that the dust formed around the star has an influence on the near-IR spectrum (Tej et al. 2003).

To study the effect of dust on the Na I and Ca I lines, the dust radiative transfer model of Groenewegen (1993) was used. In this model, the radiative transfer equation and the radiative equilibrium equation for the dust are solved simultaneously in spherical geometry (Groenewegen et al. 1994). For the dust properties we assume silicate dust (Volk & Kwok 1988) of radius $a = 0.02 \mu\text{m}$ and specific dust density of $\rho_d = 2.0 \text{ g/cm}^3$. As input model we used a blackbody with $T_{\text{eff}} = 2500$ K and with the Ca I and Na I lines imposed upon it. A dust-to-gas ratio of $\Psi = 0.01$ and an outflow velocity of $v = 15 \text{ km/s}$ were assumed. For a grid in mass-loss and dust temperature the models give an indication of the dust-influence on these lines. Typical AGB mass-loss rates (between $\dot{M} = 10^{-7} M_{\odot}/\text{yr}$ and $10^{-4} M_{\odot}/\text{yr}$) and dust temperatures ($T_{dust} = 1500, 1000$ and 750 K) were used. The model with no mass-loss is used as a reference model.

Fig. 9 shows the effect of the increasing dust amount on the equivalent line widths of Na I and Ca I. For both lines a similar trend can be seen in which the equivalent line widths decrease for increasing mass loss rates. The effect is stronger for higher dust temperatures, except at the $10^{-4} M_{\odot}/\text{yr}$ mass loss rate where the Na I and Ca I lines become undetectable

for the three dust temperatures. The effect is also stronger with increasing wavelength and impacts the Ca I more than the Na I. Unfortunately, we do not know the temperature of the dust, neither do we know the mass-loss rate for our individual sources. We can only demonstrate here the possible influence of the dust on the measured near-infrared spectrum. Surprisingly, negative values for EW(Ca) were measured for these models. This is merely due to the chosen continuum: the change in the continuum's slope is so drastic that it causes negative equivalent line width measurements.

4.3. Water content in OH/IR stars

Water absorption lines can influence the near-IR medium resolution spectra of AGB stars severely in a way which depends on the phase of the variable star as was shown in Tej et al. (2003). The high resolution spectrum of *o* Cet, a M type Mira, in Wallace & Hinkle (1996) shows that a lot of water lines are situated at wavelengths where the Ca I and Na I lines are observed. In the case of the Ca I line, the strong waterlines are situated where the continuum of the line is determined. The water lines depress the continuum in a medium resolution spectrum and make the equivalent line width measurements unreliable. For a strong enough depression of the continuum, one can expect to start to see the Ca I line apparently in emission. In the case of the Na I line, the water lines affect both the continuum and the Na I line, so that one can expect to see the EW(Na) decrease because of a smaller contrast between the continuum and the line, similar to what is seen due to the influence of the dust on the spectrum, as discussed in the previous subsection.

These effects are reflected in Fig. 10 where the EW(Ca) and the EW(Na) can be seen in comparison with our determination of the water absorption. We see that the RGB stars, with little water absorption, have higher EW(Ca) and the EW(Na) values than the LPVs and OH/IR stars. The effect seems stronger for Ca I where for EW(H_2O) below -300 \AA , we basically have no detections any more. For the Na I line the decrease is more gradual with increasing water absorption. Of course the effect of dust and other factors (such as pulsation amplitude, T_{eff}) on the spectra is also included in these figures and cannot be distinguished from the effect that the water absorption has.

4.4. Variability

Fig. 6 shows clearly the differences in the measured absorption for water for the stars we have in common with Schultheis et al. (2003). The water absorption is expected to be largely correlated with the phase for a given star: the most intense water features are to be seen at minimum light (Lançon & Wood 2000; Bessell et al. 1996; Tej et al. 2003).

Wood et al. (1998) determined periods for 80 GC OH/IR stars. We retrieved K light curves for 41 out of the 50 stars in common with our sample. The lightcurves were extrapolated using the fundamental period and the first harmonic (Wood 2004) to

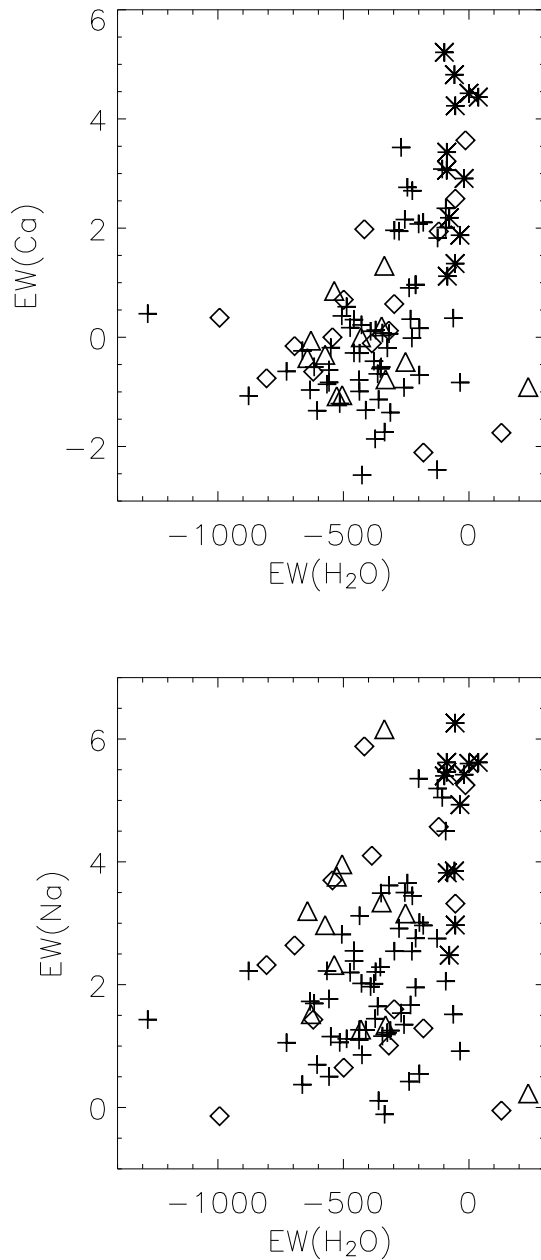


Fig. 10. Upper panel: $EW(\text{Ca})$ vs $EW(\text{H}_2\text{O})$, lower panel: $EW(\text{Na})$ vs $EW(\text{H}_2\text{O})$. The OH/IR in this work are the crosses, RGB (Schultheis et al. 2003): stars, OH/IR (Schultheis et al. 2003): diamonds, LPV (Schultheis et al. 2003): triangles. All equivalent line widths are given in the same unit \AA .

determine the phase ($= \phi$) when the star was observed in our campaign. ϕ has been calculated in a non-traditional way. We calculated ϕ such that the maximum of the lightcurve is 0 and that the minimum is always at $\phi = 0.5$. When the lightcurve reaches $\langle K \rangle$ the values of 0.25/0.75 were fixed. The other values for ϕ were then interpolated between the fixed ones (see Fig. 11).

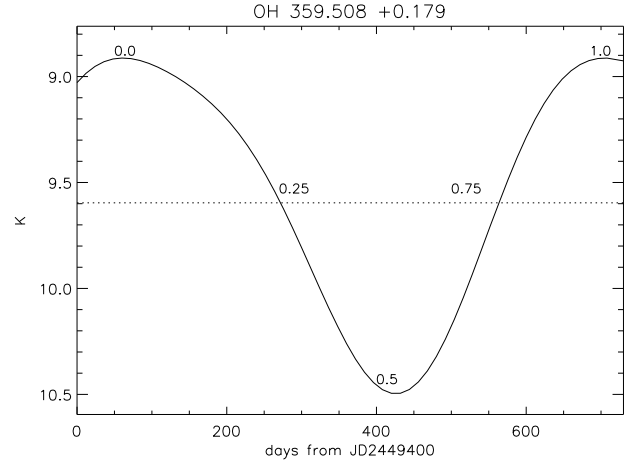


Fig. 11. Determination of the phase ϕ , $\langle K \rangle$ is represented by the dotted horizontal line.

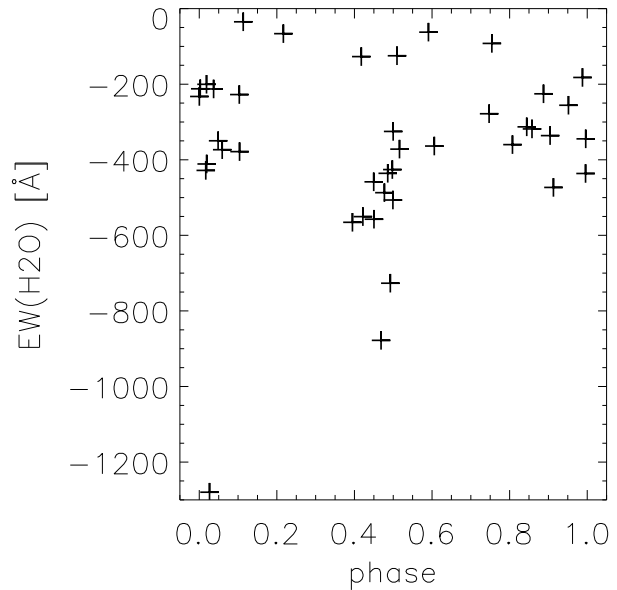


Fig. 12. The phase at time of observation versus the equivalent line width of water absorption.

Fig. 12 shows the phase ϕ versus the equivalent line width of water. The expected correlation can be seen in this figure, but not as clear as anticipated. Fig. 12 indicates that the water absorption is highest, except for one star, for $\phi = 0.5$, which indicates the light minimum. For the other phases there is a large spread and no clear trend, which can be expected as the individual stars have different parameters.

4.5. Expansion velocities

Lindqvist et al. (1992b) determined for their sample of OH/IR stars close to the GC, the expansion velocities v_{exp} . As mentioned in section 1, they divided the sample in two groups

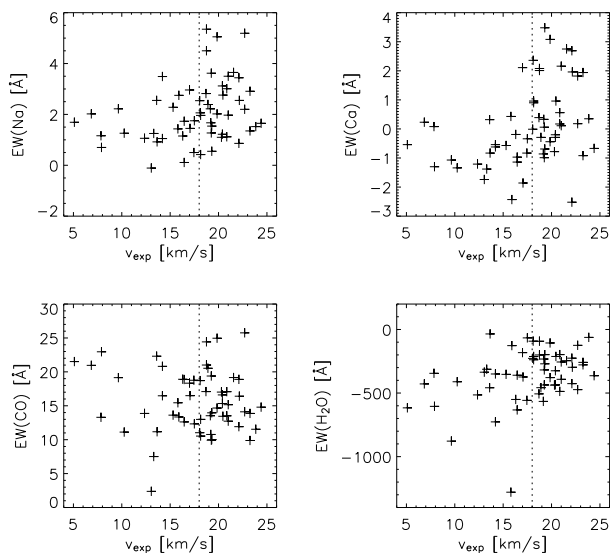


Fig. 13. Comparison of the expansion velocities with the equivalent line widths of Na I, Ca I, $^{12}\text{CO}(2,0)$ and the water absorption. The dotted vertical line separates the 2 groups of OH/IR stars.

Table 5. Mean values for the two groups of OH/IR stars.

	$v_{\text{exp}} < 18 \text{ km/s}$	$v_{\text{exp}} > 18 \text{ km/s}$
Na I	1.57 ± 0.70	2.44 ± 1.02
Ca I	-0.65 ± 0.69	0.67 ± 1.17
$^{12}\text{CO}(2,0)$	15.73 ± 3.90	15.61 ± 3.44
H ₂ O	-452.90 ± 190.82	-294.97 ± 110.31

based on the expansion velocities. The first group with the lowest expansion velocities are kinematically different and show larger dispersions in their radial velocities.

With our spectra we wanted to see whether we could find metallicity differences between the two kinematically different groups. As shown in the previous subsections, this is not possible using the relationship based on the equivalent line widths of Na I, Ca I and $^{12}\text{CO}(2,0)$ in nonvariable stars with low mass loss rates (see Ramírez et al. 2000; Frogel et al. 2001; Schultheis et al. 2003). We still wanted to investigate whether we can find differences in the equivalent line widths of the individual lines for the two groups. Fig. 13 shows, for our sample of OH/IR stars, the comparison between the expansion velocities and the equivalent line widths of Na I, Ca I, $^{12}\text{CO}(2,0)$ and the water absorption around $1.6 \mu\text{m}$. Table 5 gives the mean values with standard deviation for the measured equivalent line widths and the water indication for the both groups. Fig. 13 and Table 5 seem to indicate that the OH/IR stars in the first group have smaller EW(Na) and have a larger spread for the water absorption. Based on the numbers in Table 5 there is no difference between the EW(CO) for both groups. Concerning Ca I, the majority of the OH/IR stars in the first group have no measurable equivalent line widths. Since the water absorption

has a larger spread for this group and the dependence seen in Fig. 10 it is consistent that we measure for the majority of these stars negative EW(Ca).

Decin (2000) indicates that the linestrength of H₂O increases with decreasing metallicity. This could explain why we see stronger water absorption for the OH/IR stars in the first group, provided these OH/IR stars are older and have lower metallicities than the stars in the second group, as suggested by kinematics and outflow velocities.

5. Conclusions

We obtained near-IR data ($1.53 - 2.52 \mu\text{m}$) with SOFI on the NTT for 70 OH/IR stars located in the GC. The spectra were analysed based on the equivalent line widths of Na I, Ca I and $^{12}\text{CO}(2,0)$. The curvature of the spectrum around $1.6 \mu\text{m}$ gives us an indication of the water amount. The equivalent line widths of Na I, Ca I and $^{12}\text{CO}(2,0)$ were found to have low values in comparison to the GC static giant stars. For a large fraction of the OH/IR stars, we even found that Ca I lines could not be detected.

We discuss different aspects which can influence the determination of the equivalent line widths in the near-infrared spectra. The OH/IR stars have a variable amount of water, which influences especially the Ca I lines. The water lines just besides the Ca I line depress the continuum, causing the Ca I lines to disappear in the spectrum. The effect is also noticeable for Na I but is less strong.

We also discuss the effect of the circumstellar dust on the near-infrared spectrum. Using the radiative transfer model (Groenewegen 1993), it became clear that for the highest mass-loss rates the dust has the same effect on the Ca I and Na I lines as the water content: the lines become weaker and in the extreme case of mass loss rates in the order of $10^{-4} M_{\odot}/\text{yr}$ even disappear in the continuum and are no longer measurable. For the lower mass-loss rates ($\sim 10^{-6} M_{\odot}/\text{yr}$), the decrease of the equivalent line widths depends strongly on the dust temperature. Since we do not know the exact dust temperature and the mass-loss rates of these OH/IR stars, we cannot distinguish between the possible effects which weaken the lines.

The different effects discussed above prevent us from finding a clear distinction between the two groups of OH/IR stars.

Acknowledgements. M.S. is supported by an APART fellowship. We want to thank P.R. Wood, who kindly provided us with the K lightcurves for the OH/IR stars.

Appendix A: Tables

Appendix B: Near-IR Spectra

References

Aringer, B., Jorgensen, U. G., & Langhoff, S. R. 1997, A&A, 323, 202

Table A.4. Contribution of other species to the equivalent line width measurement of Na I. Based on Wallace & Hinkle (1996).

Na I feature	Na I continuum # 1	Na I continuum # 2
CN(0,2)	CN(0,2)	CN(0,2)
CN(1,3)	CN(1,3)	CN(1,3)
CN(2,4)	CN(2,4)	CN(2,4)
CN blend	Si	CN blend
V	Fe	
Na		
Fe		
Si		
Sc		

Table A.5. Contribution of other species to the equivalent line width measurement of Ca I. Based on Wallace & Hinkle (1996).

Ca I feature	Ca I continuum # 1	Ca I continuum # 2
CN(0,2)	CN(0,2)	CN(2,4)
CN(1,3)	CN(1,3)	HF
CN(2,4)	CN(2,4)	S
CN blend	CN blend	
Si	Si	
Sc	Fe	
Ca	V	
Ti		
Fe		
Ni		

Table A.6. Contribution of other species to the equivalent line width measurement of $^{12}\text{CO}(2,0)$. Based on Wallace & Hinkle (1996).

$^{12}\text{CO}(2,0)$ feature	$^{12}\text{CO}(2,0)$ continuum #1	$^{12}\text{CO}(2,0)$ continuum # 2
CN(0,2)	CN(0,2)	CN(0,2)
CN(1,3)	CN(2,4)	CN(1,3)
CN(2,4)	Si	CN(2,4)
Ti		CN blend
HF		Ti
CO(2,0)		HF

Baud, B., Habing, H. J., Matthews, H. E., & Winnberg, A. 1981, *A&A*, 95, 156

Bessell, M. S., Scholz, M., & Wood, P. R. 1996, *A&A*, 307, 481

Blommaert, J. A. D. L., van der Veen, W. E. C. J., & Habing, H. J. 1993, *A&A*, 267, 39

Blommaert, J. A. D. L., van der Veen, W. E. C. J., van Langevelde, H. J., Habing, H. J., & Sjouwerman, L. O. 1998, *A&A*, 329, 991

Cardelli, J. A., Clayton, G. C., & Mathis, J. S. 1989, *ApJ*, 345, 245

Cohen, M., Parker, Q. A., & Chapman, J. 2005, *MNRAS*, 357,

1189

Decin, L. 2000, Ph.D. Thesis

Elitzur, M., Ivezić, Ž., & Vinković, D. 2003, in *ASSL Vol. 283: Mass-Losing Pulsating Stars and their Circumstellar Matter*, 265–273

Frogel, J. A., Stephens, A., Ramírez, S., & DePoy, D. L. 2001, *AJ*, 122, 1896

Groenewegen, M. A. T. 1993, Ph.D. Thesis

Groenewegen, M. A. T., de Jong, T., & Gaballe, T. R. 1994, *A&A*, 287, 163

Habing, H. & Whitelock, P. 2003, in *Asymptotic giant branch stars*, by Harm J. Habing and Hans Olofsson. *Astronomy and astrophysics library*, New York, Berlin: Springer, 2003, 411–454

Habing, H. J. 1996, *A&AR*, 7, 97

Habing, H. J., Tignon, J., & Tielens, A. G. G. M. 1994, *A&A*, 286, 523

Jones, T. J., McGregor, P. J., Gehrz, R. D., & Lawrence, G. F. 1994, *AJ*, 107, 1111

Lançon, A. & Wood, P. R. 2000, *A&AS*, 146, 217

Lindqvist, M., Habing, H. J., & Winnberg, A. 1992a, *A&A*, 259, 118

Lindqvist, M., Winnberg, A., Habing, H. J., & Matthews, H. E. 1992b, *A&AS*, 92, 43

Omont, A., Gilmore, G. F., Alard, C., et al. 2003, *A&A*, 403, 975

Origlia, L., Moorwood, A. F. M., & Oliva, E. 1993, *A&A*, 280, 536

Ortiz, R., Blommaert, J. A. D. L., Copet, E., et al. 2002, *A&A*, 388, 279

Ramírez, S. V., Depoy, D. L., Frogel, J. A., Sellgren, K., & Blum, R. D. 1997, *AJ*, 113, 1411

Ramírez, S. V., Stephens, A. W., Frogel, J. A., & DePoy, D. L. 2000, *AJ*, 120, 833

Schultheis, M., Ganesh, S., Simon, G., et al. 1999, *A&A*, 349, L69

Schultheis, M., Lançon, A., Omont, A., Schuller, F., & Ojha, D. K. 2003, *A&A*, 405, 531

Sevenster, M. N., Chapman, J. M., Habing, H. J., Killeen, N. E. B., & Lindqvist, M. 1997, *A&AS*, 122, 79

Sjouwerman, L. O., van Langevelde, H. J., Winnberg, A., & Habing, H. J. 1998, *A&AS*, 128, 35

Tej, A., Lançon, A., Scholz, M., & Wood, P. R. 2003, *A&A*, 412, 481

van Langevelde, H. J., Brown, A. G. A., Lindqvist, M., Habing, H. J., & de Zeeuw, P. T. 1992, *A&A*, 261, L17

Volk, K. & Kwok, S. 1988, *ApJ*, 331, 435

Wallace, L. & Hinkle, K. 1996, *ApJS*, 107, 312

Wood, P. R. 2004, private communication

Wood, P. R., Habing, H. J., & McGregor, P. J. 1998, *A&A*, 336, 925

Wood, P. R., Whiteoak, J. B., Hughes, S. M. G., et al. 1992, *ApJ*, 397, 552

List of Objects

‘OH 359.576 +0.091’ on page 12

‘OH 359.598 +0.000’ on page 12
 ‘OH 359.669 -0.019’ on page 12
 ‘OH 359.675 +0.069’ on page 12
 ‘OH 359.678 -0.024’ on page 12
 ‘OH 359.681 -0.095’ on page 12
 ‘OH 359.711 -0.100’ on page 12
 ‘OH 359.748 +0.274’ on page 12
 ‘OH 359.755 +0.061’ on page 12
 ‘OH 359.757 -0.136’ on page 12
 ‘OH 359.762 +0.120’ on page 12
 ‘OH 359.765 +0.082’ on page 12
 ‘OH 359.768 -0.207’ on page 12
 ‘OH 359.783 -0.392’ on page 12
 ‘OH 359.797 -0.025’ on page 12
 ‘OH 359.799 -0.090’ on page 12
 ‘OH 359.800 +0.165’ on page 12
 ‘OH 359.803 -0.248’ on page 12
 ‘OH 359.810 -0.070’ on page 12
 ‘OH 359.825 -0.024’ on page 12
 ‘OH 359.837 +0.030’ on page 12
 ‘OH 359.838 +0.053’ on page 12
 ‘OH 359.889 +0.361’ on page 12
 ‘OH 359.906 -0.041’ on page 12
 ‘OH 359.943 +0.260’ on page 12
 ‘OH 0.001 +0.352’ on page 12
 ‘OH 0.019 +0.345’ on page 12
 ‘OH 0.138 -0.136’ on page 12
 ‘OH 0.173 +0.211’ on page 12
 ‘OH 0.200 +0.233’ on page 12
 ‘OH 0.221 +0.168’ on page 12
 ‘HD 130223’ on page 12
 ‘HD 133336’ on page 12
 ‘HD 181012’ on page 12
 ‘HD 224715’ on page 12
 ‘WX Psc’ on page 12
 ‘OH 359.437 -0.051’ on page 13
 ‘OH 359.508 +0.179’ on page 13
 ‘OH 359.513 +0.174’ on page 13
 ‘OH 359.634 -0.195’ on page 13
 ‘OH 359.636 -0.108’ on page 13
 ‘OH 359.640 -0.084’ on page 13
 ‘OH 359.684 -0.104’ on page 13
 ‘OH 359.716 -0.070’ on page 13
 ‘OH 359.719 +0.025’ on page 13
 ‘OH 359.760 +0.072’ on page 13
 ‘OH 359.763 -0.042’ on page 13
 ‘OH 0.018 +0.156’ on page 13
 ‘OH 0.036 -0.182’ on page 13
 ‘OH 0.040 -0.056’ on page 13
 ‘OH 0.060 -0.018’ on page 13
 ‘OH 0.076 +0.146’ on page 13
 ‘OH 0.129 +0.103’ on page 13
 ‘OH 0.142 +0.026’ on page 13
 ‘OH 0.178 -0.055’ on page 13
 ‘OH 0.225 -0.055’ on page 13
 ‘OH 0.241 -0.014’ on page 13
 ‘OH 0.265 -0.078’ on page 13
 ‘OH 0.274 +0.086’ on page 13
 ‘OH 0.307 -0.176’ on page 13
 ‘OH 0.336 -0.027’ on page 13
 ‘HD 109467’ on page 13
 ‘HD 115141’ on page 13
 ‘HD 117927’ on page 13
 ‘HD 121870’ on page 13
 ‘AFGL 1686’ on page 13
 ‘R Phe’ on page 13
 ‘S Phe’ on page 13
 ‘SV Tel’ on page 13
 ‘U Equ’ on page 13
 ‘Z Aql’ on page 13
 ‘OH 359.746 +0.134’ on page 14
 ‘OH 359.778 +0.010’ on page 14
 ‘OH 359.814 -0.162’ on page 14
 ‘OH 359.836 +0.119’ on page 14
 ‘OH 359.855 -0.078’ on page 14
 ‘OH 359.864 +0.056’ on page 14
 ‘OH 359.918 -0.055’ on page 14
 ‘OH 359.943 -0.055’ on page 14
 ‘OH 0.017 +0.156’ on page 14
 ‘OH 0.037 -0.003’ on page 14
 ‘OH 0.335 -0.180’ on page 14
 ‘OH 0.352 +0.175’ on page 14
 ‘OH 0.379 +0.159’ on page 14
 ‘OH 0.395 +0.008’ on page 14
 ‘OH 0.447 -0.006’ on page 14
 ‘OH 0.452 +0.046’ on page 14
 ‘OH 0.536 -0.130’ on page 14
 ‘BMB 55’ on page 14
 ‘B-138’ on page 14
 ‘BMB 205’ on page 14
 ‘BMB 78’ on page 14
 ‘BMB 289’ on page 14
 ‘B-124’ on page 14
 ‘OH 359.437-0.051’ on page 15
 ‘OH 359.803-0.248’ on page 16
 ‘OH 359.943-0.055’ on page 17
 ‘OH 0.452+0.046’ on page 18

Table A.1. Log of the stars observed on 28/06/03.

Name	RA	Dec	References ^a	EW(Na) [Å]	EW(Ca) [Å]	EW(CO) [Å]	H ₂ O [Å]	P ^b [days]	v _{exp} [m/s]
OH 359.576 +0.091	17 44 57.80	-29 20 42.5	Li012, A29	2.50	0.47	15.13		672.0	18.6
OH 359.598 +0.000	17 44 39.71	-29 16 46.1	Li014, A10	1.67	0.33	10.77	-232.39	664.0	19.2
OH 359.669 -0.019	17 44 54.16	-29 13 44.9	Li020, A23	0.50	-0.83	18.76	-557.33	481.0	17.5
OH 359.675 +0.069	17 44 34.33	-29 10 38.6	Li021, A07, B98, S98	5.35	2.08	24.42	-200.35	698.0	18.8
OH 359.678 -0.024	17 44 56.83	-29 13 25.5	Li022, B98	3.65	2.75	19.16	-245.18		21.5
OH 359.681 -0.095	17 45 16.43	-29 15 37.6	Li023, A51, S98	2.76	2.78	17.01	-43.64	759.0	19.3
OH 359.711 -0.100	17 45 19.26	-29 14 01.1	Li025, A58, S98	3.62	0.06	19.39	-318.34	686.0	19.2
OH 359.748 +0.274	17 43 57.05	-29 00 28.4	Li030	-0.11	-1.74	2.38	-335.99	437.0	13.1
OH 359.755 +0.061	17 44 47.94	-29 06 49.9	Li031, A14, B98, S98	4.50	2.01	21.01	-92.73	0.0	18.8
OH 359.757 -0.136	17 45 34.41	-29 12 54.1	Sj002, A71, S98	1.10	-0.78	17.02	-437.67		20.3
OH 359.762 +0.120	17 44 34.96	-29 04 35.7	Li033, B98, E51, S98	2.28	-0.57	13.62	-352.97		15.3
OH 359.765 +0.082	17 44 44.43	-29 05 37.9	Li035, A12, S98	2.75	-2.43	13.35	-126.89	552.0	15.9
OH 359.768 -0.207	17 45 52.62	-29 14 30.4	Li036	1.27	-0.99	9.92	-436.23	602.0	19.2
OH 359.783 -0.392	17 46 38.12	-29 19 30.7	Li039	1.25	-1.38	7.51	-312.88	559.0	13.3
OH 359.797 -0.025	17 45 14.27	-29 07 20.8	Sj004, A52, S98	1.54	3.48	13.96	-269.95		19.3
OH 359.799 -0.090	17 45 29.50	-29 09 16.0	Li040, B98, S98	1.11	-0.51	15.97			18.1
OH 359.800 +0.165	17 44 30.11	-29 01 14.3	Li041	3.49	-0.54	16.47	-349.81	461.0	14.2
OH 359.803 -0.248	17 46 07.10	-29 13 56.1	Li043, S98	4.72	3.94	20.13	-25.58	803.0	18.5
OH 359.810 -0.070	17 45 26.35	-29 08 03.9	Li044, A64, B98, S98	2.55	1.96	16.41	-297.19		22.1
OH 359.825 -0.024	17 45 17.83	-29 05 53.3	Li047, B98, S98	0.37	-0.25	19.95	-663.81		
OH 359.837 +0.030	17 45 06.98	-29 03 34.9	Li048, A43, B98, S98	1.16	0.08	13.30	-344.67	402.0	7.8
OH 359.838 +0.053	17 45 01.70	-29 02 49.9	Sj011, A36	1.06	-1.21	13.87	-514.62		12.4
OH 359.889 +0.361	17 43 56.94	-28 50 30.8	Li054	2.54	-0.01	11.03	-227.34	389.0	18.1
OH 359.906 -0.041	17 45 33.17	-29 02 18.4	B98, S98	5.05	3.08	24.96	-106.08		19.8
OH 359.943 +0.260	17 44 28.17	-28 50 55.8	Li064, B98, S98	1.75	-0.34	12.33	-66.26	692.0	17.5
OH 0.001 +0.352	17 44 14.95	-28 45 06.0	Li076, S98	2.22	-1.07	19.15	-877.91	477.0	9.7
OH 0.019 +0.345	17 44 19.23	-28 44 21.8	Li079	1.52	0.35	11.54	-62.35	701.0	23.9
OH 0.138 -0.136	17 46 28.71	-28 53 19.5	Li094, S98	3.12	-0.29	16.60	-435.76	622.0	20.4
OH 0.173 +0.211	17 45 12.45	-28 40 44.4	Li096, S98	1.45	-1.86	16.49	-373.41	514.0	17.0
OH 0.200 +0.233	17 45 11.44	-28 38 43.2	Li101	1.43	0.43	15.44	-1279.67	825.0	15.8
OH 0.221 +0.168	17 45 29.02	-28 39 38.5	Li104	2.22	-0.86	13.53	-565.55	697.0	19.2
HD 130223	14 47 53.62	-32 14 49.5	R97	2.72	2.48	17.25	-11.74		
HD 133336	15 04 52.37	-31 16 44.7	R97	2.32	2.37	15.65	-11.83		
HD 181012	19 20 13.43	-36 13 39.8	R97	2.10	2.21	17.63	-17.89		
HD 224715	00 00 09.82	-35 57 36.8	R97	1.84	2.04	14.44	-33.38		
WX Psc	01 06 25.98	+12 35 53.0	L00	2.10	0.65	15.06	-290.88		

^a Li: Lindqvist et al. (1992b), Sj: Sjouwerman et al. (1998) and Ortiz et al. (2002), B98: Blommaert et al. (1998), A: Schultheis et al. (2003), HV: van Langevelde et al. (1992), R97: Ramírez et al. (1997), R00: Ramírez et al. (2000), L00: Lançon & Wood (2000), and S98: Sjouwerman et al. (1998).

^b Periods are taken from Wood et al. (1998).

Table A.2. Log of the stars observed on 29/06/03.

Name	RA	Dec	References ^a	EW(Na) [Å]	EW(Ca) [Å]	EW(CO) [Å]	H ₂ O [Å]	P ^b [days]	v _{exp} [m/s]
OH 359.437 -0.051	17 44 28.30	-29 26 35.0	Li004	4.77	3.05	19.80	-45.15	0.0	15.3
OH 359.508 +0.179	17 43 44.74	-29 15 44.6	Li009	2.02	-0.44	14.67	-378.36	644.0	19.8
OH 359.513 +0.174	17 43 46.73	-29 15 38.4	Li010	1.26	-1.34	11.12	-411.05	461.0	10.2
OH 359.634 -0.195	17 45 30.45	-29 21 00.0	Li016	2.21	0.13	15.22	-371.80	501.0	0.0
OH 359.636 -0.108	17 45 10.39	-29 18 12.3	Li017	0.86	-2.52	11.92	-425.97	847.0	22.1
OH 359.640 -0.084	17 45 05.29	-29 17 13.4	Li018	2.55	0.32	22.31	-458.27	546.0	13.6
OH 359.684 -0.104	17 45 16.43	-29 15 37.6	Li024, S98	1.15	-0.19	18.91	-550.36	535.0	16.3
OH 359.716 -0.070	17 45 13.00	-29 12 54.0	Li026, S98	5.19	1.82	25.75	-124.72	691.0	22.7
OH 359.719 +0.025	17 44 51.25	-29 09 45.3	Li027	2.20	0.18	14.11	-473.12	669.0	22.7
OH 359.760 +0.072	17 44 45.96	-29 06 13.6	Li032	1.12	0.56	17.08	-487.08	676.0	20.9
OH 359.763 -0.042	17 45 13.07	-29 09 36.3	Li034, S98	1.05	-0.62	20.81	-726.67	453.0	14.2
OH 0.018 +0.156	17 45 03.30	-28 50 22.0	Li078, S98	2.02	0.23	20.96	-428.16	423.0	6.9
OH 0.036 -0.182	17 46 24.87	-29 00 01.4	Li080, S98	1.98	-1.61	7.64	-4085.92	660.0	18.8
OH 0.040 -0.056	17 45 56.08	-28 55 52.0	B98, S98	3.01	0.17	13.52	-197.38		20.8
OH 0.060 -0.018	17 45 50.07	-28 53 38.1	B98	0.55	-0.69	10.01	-197.71		19.3
OH 0.076 +0.146	17 45 13.91	-28 47 43.2	Li086, B98, S98	1.97	0.11	12.73	-391.78		21.0
OH 0.129 +0.103	17 45 31.45	-28 46 22.1	Li091, B98, S98	1.77	-0.60	21.15	-557.53		
OH 0.142 +0.026	17 45 51.33	-28 48 06.8	B98	1.35	-0.92	9.88	-258.59		23.2
OH 0.178 -0.055	17 46 13.85	-28 48 50.4	B98	1.73	-0.97	18.87	-632.77		16.5
OH 0.225 -0.055	17 46 22.11	-28 46 22.6	Li105, B98	0.11	-1.14	12.62	-359.80	521.0	16.5
OH 0.241 -0.014	17 46 14.96	-28 44 17.3	Li106	2.82	0.39	17.09	-506.51	535.0	18.7
OH 0.265 -0.078	17 46 33.12	-28 45 00.7	Li108	2.06	2.36	18.71	-92.13	595.0	18.1
OH 0.274 +0.086	17 45 56.08	-28 39 27.5	Li109	1.65	-0.67	14.80	-363.65	706.0	24.4
OH 0.307 -0.176	17 47 02.17	-28 45 55.8	Li110	1.22	-0.20	15.33	-324.90	657.0	20.4
OH 0.336 -0.027	17 46 31.30	-28 39 48.0	Li113	2.96	2.11	18.33	-182.05	514.0	17.0
HD 109467	12 35 04.30	-28 46 39.6	R97	2.73	1.84	17.68	-15.21		
HD 115141	13 15 49.54	-40 03 17.1	R97	0.93	0.29	7.28	-8.41		
HD 117927	13 34 15.34	-34 23 15.3	R97	0.90	0.19	6.03	-2.47		
HD 121870	13 58 53.01	-32 47 32.5	R97	2.87	1.69	17.03	-24.24		
AFGL 1686	14 11 17.61	-07 44 49.9	L00	1.96	-0.79	18.87	-528.16		
R Phe	23 56 27.57	-49 47 12.5	L00	1.86	0.23	12.89	-118.80		
S Phe	23 59 04.57	-56 34 32.3	L00	2.17	1.48	17.56	-15.30		
SV Tel	18 56 17.94	-49 29 09.7	L00	-1.20	0.29	11.69	-481.43		
U Equ	20 57 16.28	+02 58 44.6	L00	-1.65	0.70	-2.35	-109.43		
Z Aql	20 15 11.04	-06 09 04.0	L00	0.12	0.53	12.65	-201.51		

^a See Table A.1.^b See Table A.1.

Table A.3. Log of the stars observed on 30/06/03.

Name	RA	Dec	References ^a	EW(Na) [Å]	EW(Ca) [Å]	EW(CO) [Å]	H ₂ O [Å]	P ^b [days]	v _{exp} [m/s]
OH 359.746 +0.134	17 44 29.42	-29 04 58.6	Li029, S98	0.70	-1.30	22.96	-604.71		7.9
OH 359.778 +0.010	17 45 03.20	-29 07 12.6	Li038, S98	3.50	2.16	15.16	-255.61	557.0	21.0
OH 359.814 -0.162	17 45 48.48	-29 10 45.2	Li045, S98	2.76	0.96	13.45	-212.24	554.0	20.5
OH 359.836 +0.119	17 44 45.97	-29 00 50.9	Sj009, HV	-1.31	1.01	14.06	-126.84		
OH 359.855 -0.078	17 45 34.79	-29 06 02.7	Li050	3.44	2.69	18.89	-225.50	617.0	22.1
OH 359.864 +0.056	17 45 04.71	-29 01 24.9	Sj013, A38, HV	0.09	0.57	22.89	-660.83		
OH 359.918 -0.055	17 45 38.46	-29 02 03.9	B98, S98	0.42	0.90	10.53	-238.09		18.1
OH 359.943 -0.055	17 44 28.20	-28 50 55.0	S98	2.49	1.66	14.73	31.60		
OH 0.017 +0.156	17 45 03.65	-28 50 27.7	S98	2.39	-0.29	20.53	-457.78		18.9
OH 0.037 -0.003	17 45 43.16	-28 54 21.8	S98	1.69	-0.54	21.52	-616.51		5.1
OH 0.335 -0.180	17 47 07.34	-28 44 28.3	HV, S98	3.33	1.65	17.06	-2.82		
OH 0.352 +0.175	17 45 46.57	-28 32 39.5	Li115	1.96	0.96	12.99	-212.56	661.0	18.1
OH 0.379 +0.159	17 45 54.18	-28 31 46.0	Li116	3.48	-0.37	2.75		985.0	15.3
OH 0.395 +0.008	17 46 31.48	-28 35 37.3	Li117	0.92	-0.83	11.17	-34.99	461.0	13.7
OH 0.447 -0.006	17 46 42.29	-28 33 26.1	Li120	-0.33	-9.57	14.46		445.0	13.1
OH 0.452 +0.046	17 46 30.70	-28 31 31.0	Li121	1.96	1.47	14.14	-36.33	339.0	10.2
OH 0.536 -0.130	17 47 24.02	-28 32 42.9	Li127	2.91	1.94	13.87	-278.26	669.0	23.2
	17 44 23.80	-29 08 55.3	A03	5.07	2.53	18.98	-10.57		
	17 44 48.60	-29 00 13.2	A16	6.46	1.16	20.84	-5.45		
	17 44 53.10	-28 59 46.5	A22	5.28	4.07	18.13	-6.80		
	17 45 09.80	-29 05 17.8	A45	3.28	0.68	16.53	-55.01		
	17 45 27.50	-29 04 39.9	A66	5.39	4.18	25.26	-58.05		
BMB 55	18 03 08.16	-29 57 47.4	R00	3.42	2.31	19.45	-90.37		
B-138	18 03 46.00	-29 59 12.1	R00	4.40	2.61	21.97	-48.03		
BMB 205	18 03 54.85	-30 04 19.2	R00	4.04	3.05	21.95	-57.11		
BMB 78	18 03 15.54	-29 51 09.0	R00	2.62	2.36	18.30	-28.21		
BMB 289	18 04 22.72	-29 54 50.6	R00	3.54	2.78	22.39	-111.15		
B-124	18 04 43.73	-30 05 15.3	R00	3.25	2.60	19.47	-33.46		

^a See Table A.1.^b See Table A.1.

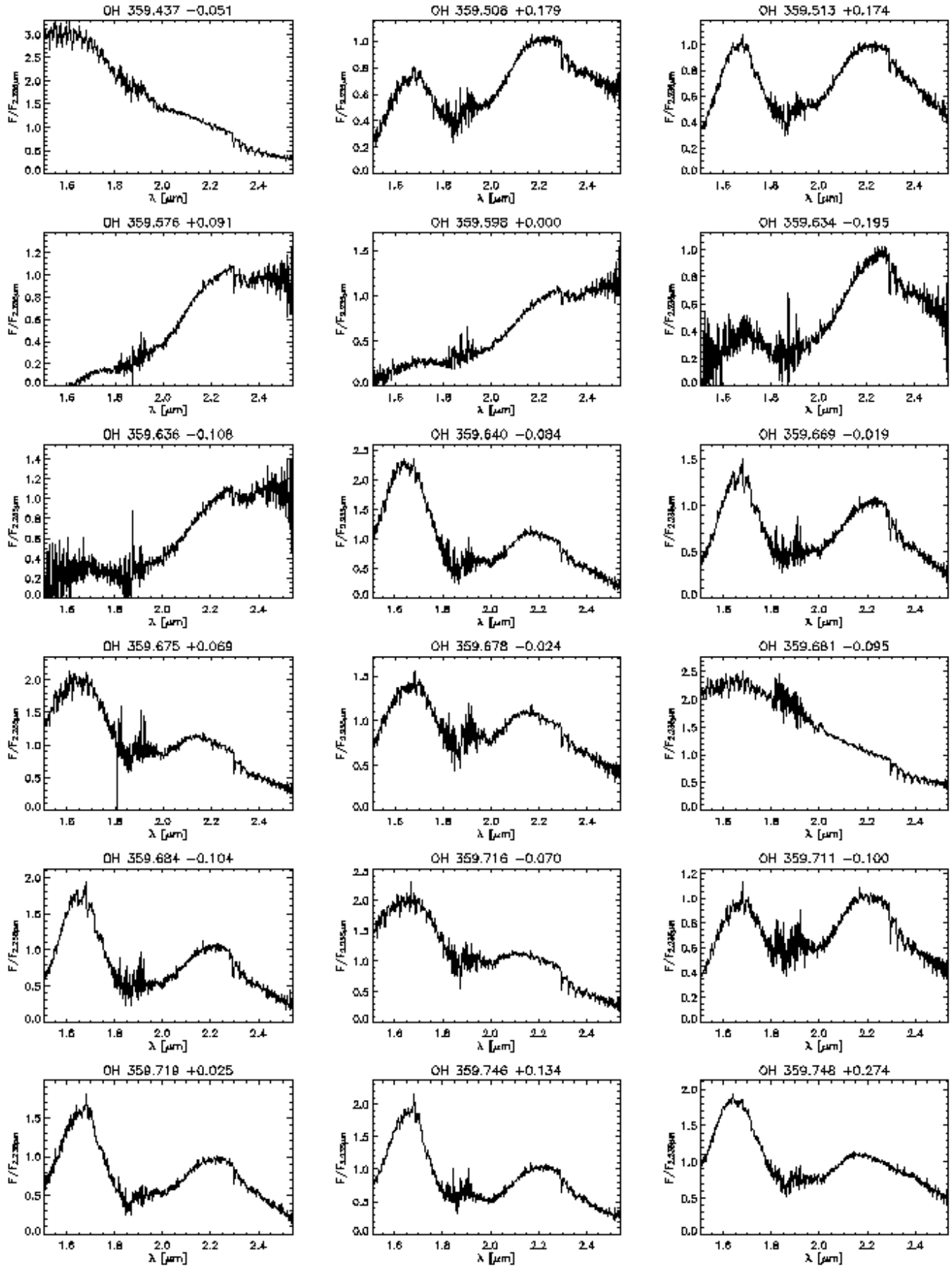


Fig. B.1. OH/IR stars. OH 359.437-0.051 is possibly a mismatch.

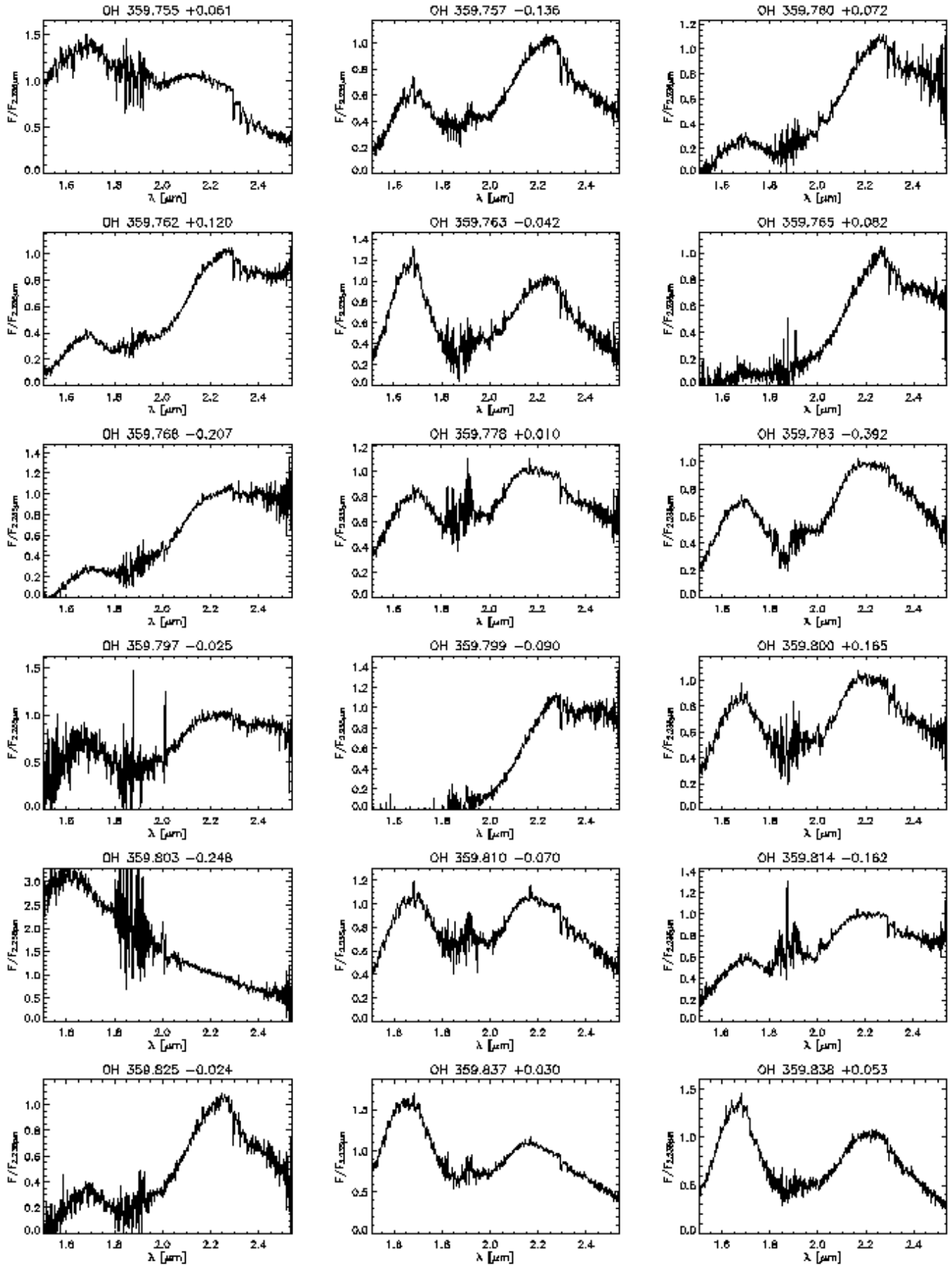


Fig. B.2. OH/IR stars - continue. OH 359.803-0.248 is possibly a mismatch.

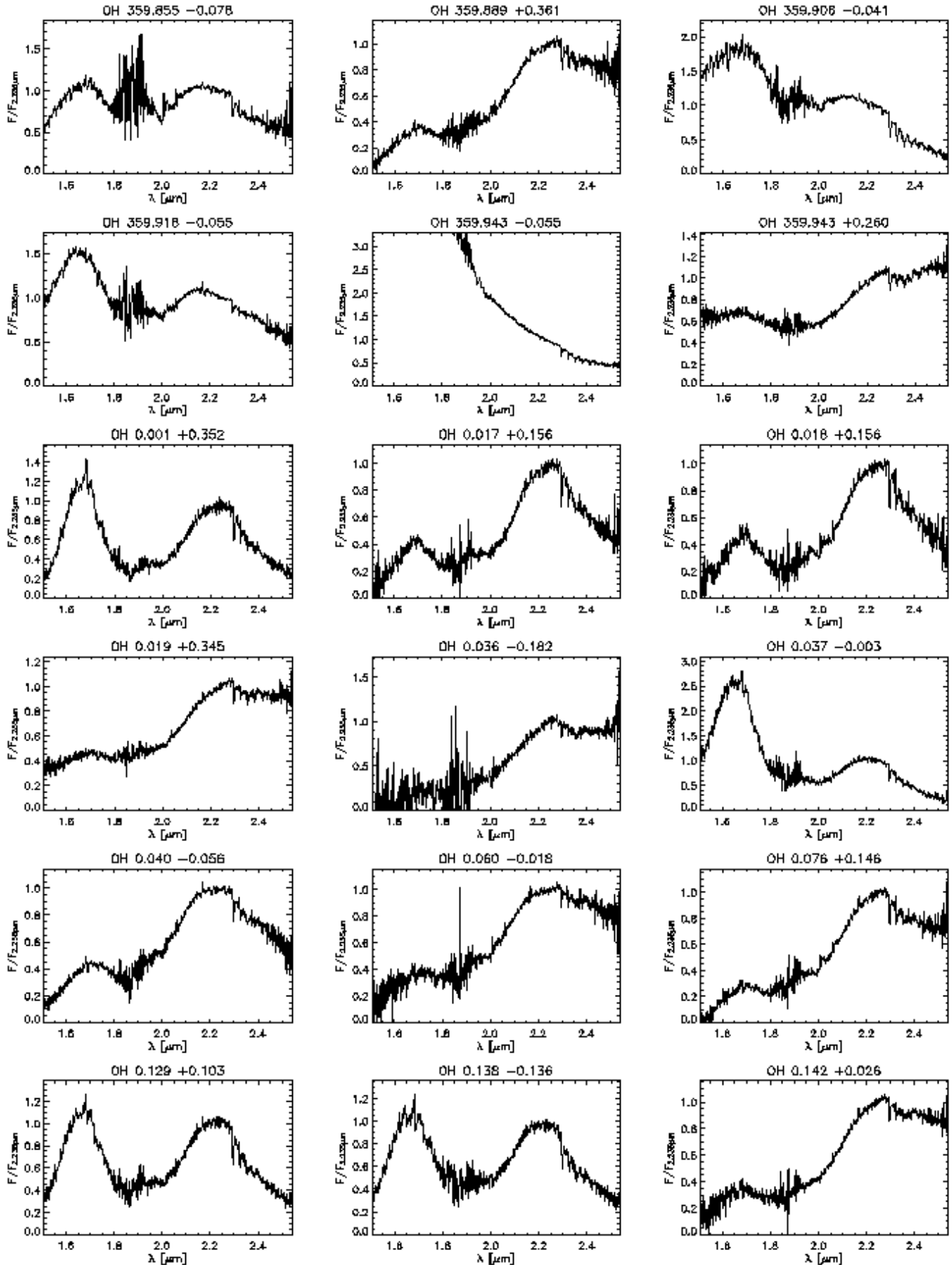


Fig. B.3. OH/IR stars - continue. OH 359.943-0.055 is possibly a mismatch.

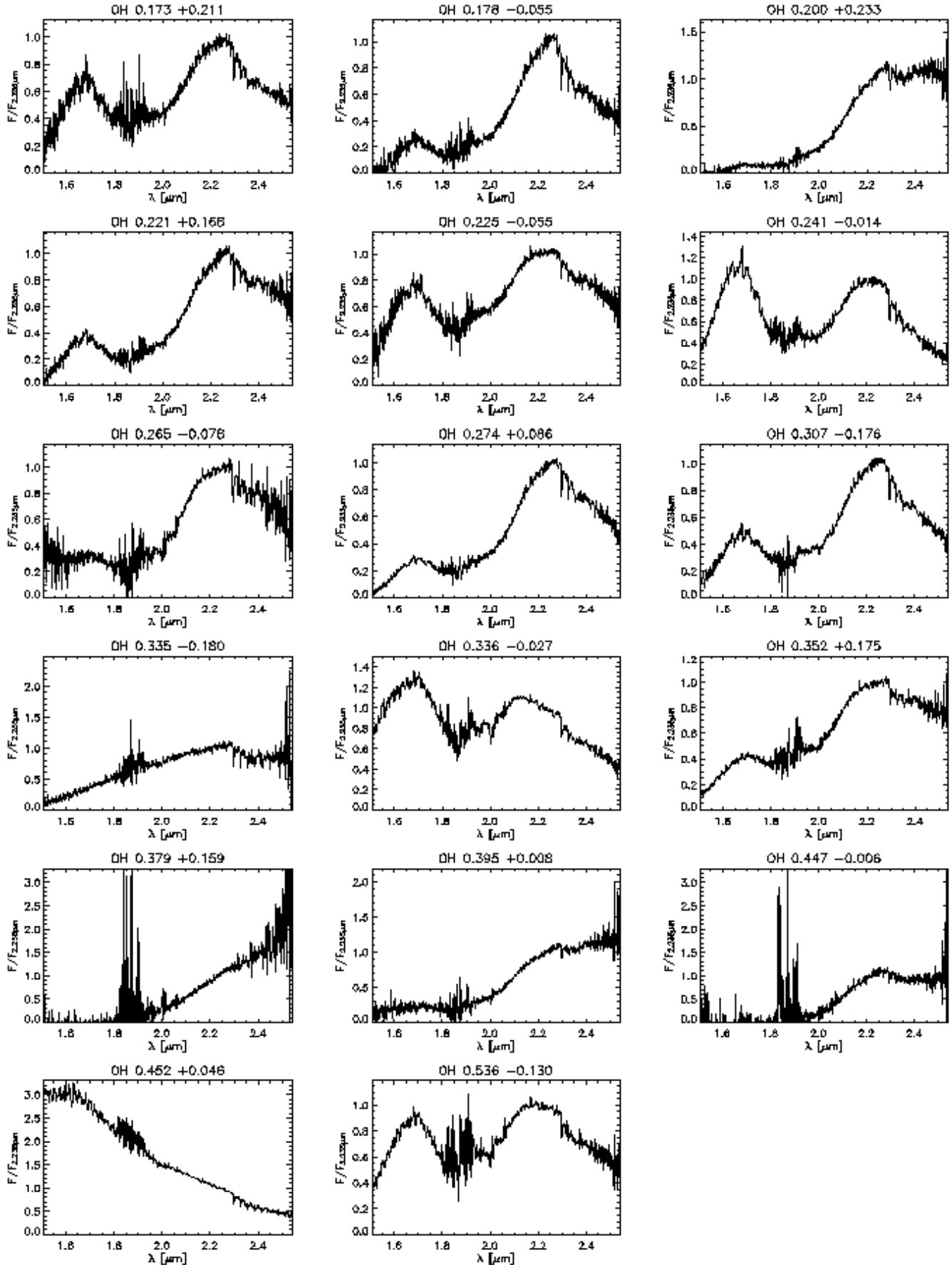


Fig. B.4. OH/IR stars - continue. OH 0.452+0.046 is possibly a mismatch.

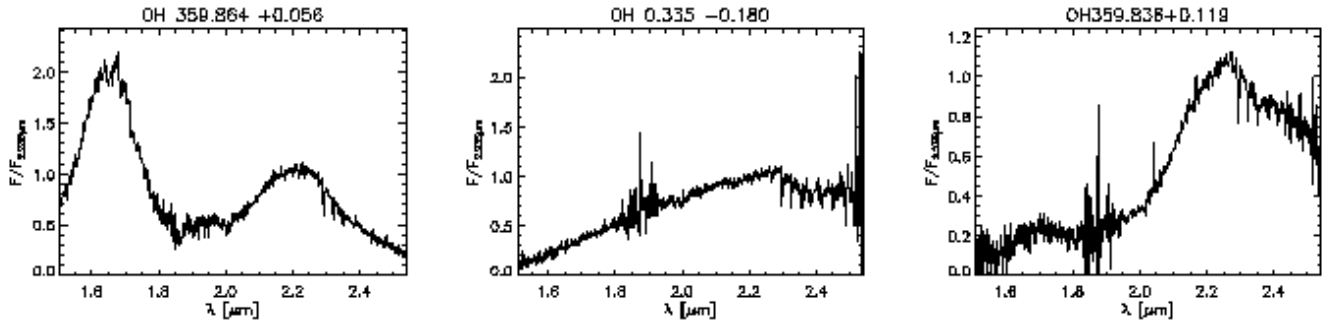


Fig. B.5. High velocity OH/IR stars (van Langevelde et al. 1992).

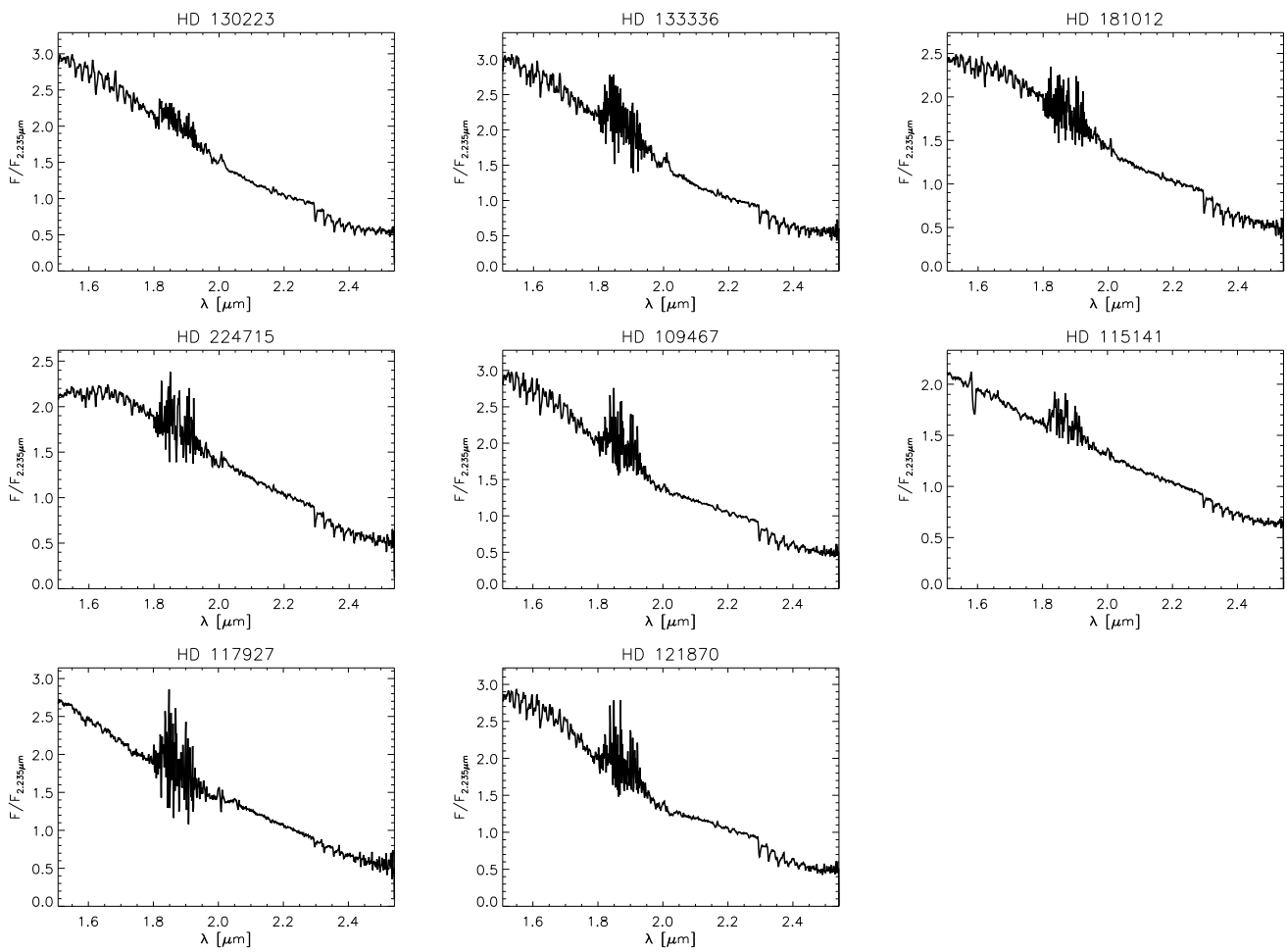


Fig. B.6. Stars in common with Ramírez et al. (1997).

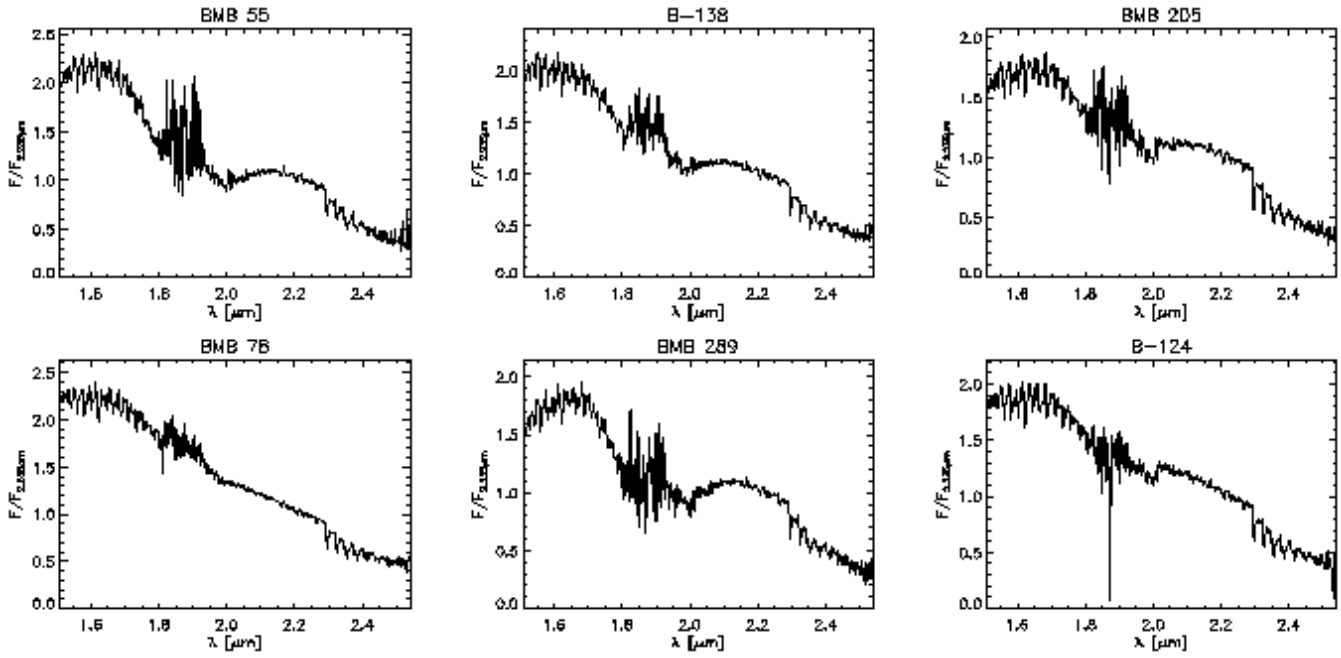


Fig. B.7. Stars in common with Ramírez et al. (2000).

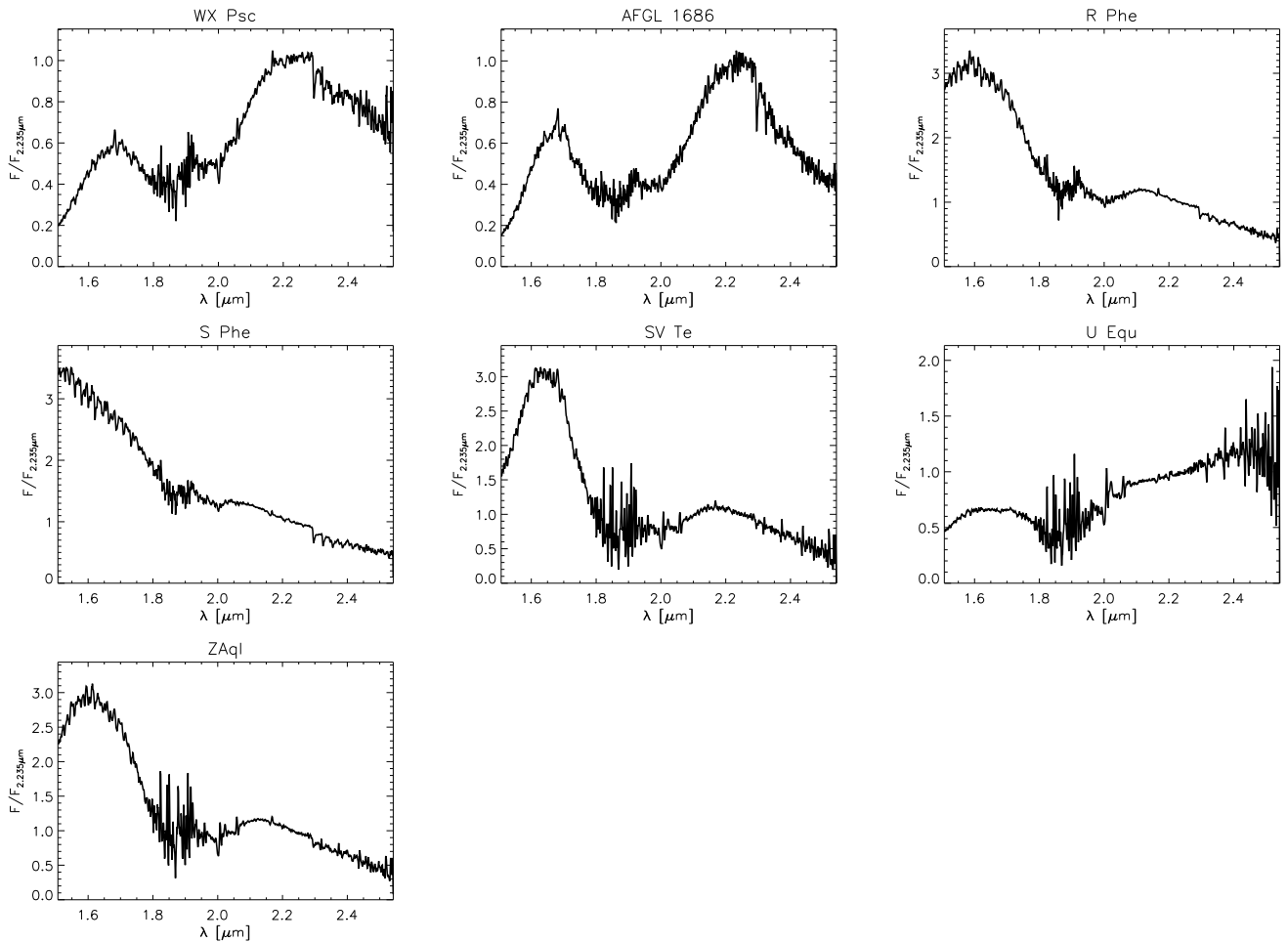


Fig. B.8. Stars in common with Lançon & Wood (2000).